

Strongly anisotropic spin dynamics in magnetic topological insulators

A. Alfonsov,^{1,*} J. I. Facio,^{1,*} K. Mehawat,^{1,2,*} A. G. Moghaddam,^{1,3} R. Ray,¹ A. Zeugner,⁴ M. Richter,^{1,5} J. van den Brink,^{1,2} A. Isaeva,^{1,2} B. Büchner,^{1,2} and V. Kataev¹

¹Leibniz IFW Dresden, D-01069 Dresden, Germany

²Institute for Solid State and Materials Physics and Würzburg-Dresden Cluster of Excellence ct.qmat, TU Dresden, D-01062 Dresden, Germany

³Department of Physics, Institute for Advanced Studies in Basic Sciences (IASBS), Zanjan 45137-66731, Iran

⁴Faculty of Chemistry and Food Chemistry, TU Dresden, D-01062 Dresden, Germany.

⁵Dresden Center for Computational Materials Science (DCMS), TU Dresden, 01062 Dresden, Germany

(Dated: April 13, 2021)

The recent discovery of magnetic topological insulators has opened new avenues to explore exotic states of matter that can emerge from the interplay between topological electronic states and magnetic degrees of freedom, be it ordered or strongly fluctuating. Motivated by the effects that the dynamics of the magnetic moments can have on the topological surface states, we investigate the magnetic fluctuations across the $(\text{MnBi}_2\text{Te}_4)(\text{Bi}_2\text{Te}_3)_n$ family. Our paramagnetic electron spin resonance experiments reveal contrasting Mn spin dynamics in different compounds, which manifests in a strongly anisotropic Mn spin relaxation in MnBi_2Te_4 while being almost isotropic in MnBi_4Te_7 . Our density-functional calculations explain these striking observations in terms of the sensitivity of the local electronic structure to the Mn spin-orientation, and indicate that the anisotropy of the magnetic fluctuations can be controlled by the carrier density, which may directly affect the electronic topological surface states.

Introduction. The experimental discovery of antiferromagnetic topological insulators (AFTIs) in the van der Waals $(\text{MnBi}_2\text{Te}_4)(\text{Bi}_2\text{Te}_3)_n$ family [1, 2] has provided a fertile new basis for the investigation of exotic phenomena rooted in the interplay between topology of the electronic structure and spontaneous symmetry breaking, such as the quantum anomalous Hall effect, the topological magnetoelectric effect and chiral Majorana fermions [3–7]. The two compounds studied the most so far, MnBi_2Te_4 and MnBi_4Te_7 , order antiferromagnetically with the A-type spin structure at Néel temperatures $T_N \sim 24\text{ K}$ and $T_N \sim 13\text{ K}$, respectively [8–14]. In this phase, both the time-reversal (Θ) and a primitive-lattice translational ($T_{1/2}$) symmetries are broken but their combination $S = \Theta T_{1/2}$ is preserved [15]. For temperatures T below T_N , the topological protection of the surface states depends on whether or not the surface is S -symmetric. At higher T , even if S can be broken locally and temporarily, the surface spectrum is expected to be gapless for any surface due to the restoration of Θ in a statistical sense [16, 17], Θ being an average symmetry. As it results from averaging over magnetic fluctuations, the interplay between these and the topological electronic surface states naturally depends on space and time scales.

Experimentally, surface states with an origin in the band inversion have been widely observed [1, 2, 12–14, 18–28] but the details around the Dirac point are subject of controversy. In particular, among experiments that show a gapped surface spectrum for $T < T_N$, whether the gap persists above T_N represents an important open question. Our previous experimental results suggested that the dynamics of the bulk localized Mn magnetic moments play a key role in MnBi_2Te_4 [1] as

electron spin resonance (ESR) measurements at $T > T_N$ show that the relaxation of the Mn moments due to the exchange coupling with the conduction electrons is strongly anisotropic. This suggests a strong anisotropy of Mn spin fluctuations which may give rise to an instantaneous (on the timescale of ESR) polarization field at the surface, preventing the gap to close even at $T \gg T_N$ as observed on the much faster timescale of the ARPES experiment. Indeed further recent work proposes that the topological gap above T_N remains open due to short-range magnetic fields generated by chiral spin fluctuations [29].

Certainly, firm and final establishment of a correspondence between the characteristics of the magnetic fluctuations of both, conduction electrons and paramagnetic Mn spins, and the surface gap is a formidable task given the current, rather unsettled, experimental situation with regard to the surface band structure in different ARPES experiments triggering different, sometimes controversial, interpretations. In this context it is of a paramount importance to unravel in detail the nature of the magnetic fluctuations across the $(\text{MnBi}_2\text{Te}_4)(\text{Bi}_2\text{Te}_3)_n$ family, the understanding of which is currently lacking. In this paper, we address this particularly crucial issue. First, we present ESR results which show that the anisotropy of the Mn spin relaxation rate in the paramagnetic state varies enormously in the family being unprecedentedly large in MnBi_2Te_4 and nearly vanishing in MnBi_4Te_7 . Second, based on density-functional calculations, we identify a critical role for the Mn spin dynamics played by the magnetic anisotropy of the electronic structure, which consistently explains the ESR data and further suggests that in doped semiconductors the car-

rier density can be used to tune the high-temperature anisotropy of the spin dynamics.

ESR experimental results. Electron spin resonance (ESR) measurements on high-quality MnBi_2Te_4 and MnBi_4Te_7 single crystalline samples synthesized and thoroughly characterized by X-ray diffraction and electron-dispersive X-ray spectroscopy in Refs. [30] and [13], respectively, were carried out at a microwave frequency of $\nu = 9.56$ GHz and at temperatures from 4 to 300 K using a commercial Bruker X-band spectrometer. The magnetic field H was swept from 0 to 9 kOe. The ESR signals have a well-defined asymmetric Dysonian shape [31, 32], typical for conducting samples. This is indeed expected since Mn/Bi antisite intermixing is omnipresent in MnBi_2Te_4 ($\text{Mn}_{0.85}\text{Bi}_{2.1}\text{Te}_4$) and MnBi_4Te_7 ($\text{Mn}_{0.8}\text{Bi}_{4.1}\text{Te}_7$) crystals and acts as intrinsic self-doping [1, 10, 11, 13, 30, 33]. Characteristic spectra are presented in Fig. 1(a),(b). At high temperature, the line shape gets somewhat distorted due to an emerging small and narrow impurity peak which can be easily taken into account in the Dysonian fit. In order to precisely align the samples in the magnetic field parallel ($H \parallel c$) and normal ($H \parallel ab$) to the c axis, we have measured the angular dependence of the linewidth (ΔH) and of the resonance field (H_{res}) at a low temperature, which are exemplarily plotted in Fig. 1(c). They follow a typical $\Delta H \sim [1 + \cos^2(\theta)]$ (or $H_{\text{res}} \sim [1 + \sin^2(\theta)]$) dependence whose extrema correspond to the respective field geometries, as indicated in the Figure.

The T -dependence of H_{res} and of ΔH obtained from the Dysonian fits are shown for both field orientations on Fig. 1(d) for MnBi_2Te_4 and on Fig. 1(e) for MnBi_4Te_7 . Due to a decrease of the intensity of the ESR signal with increasing temperature according to the Curie-Weiss law, the error bars of the fit increase correspondingly.

One can identify in Figs. 1(d),(e) a crossover temperature $T^* \sim 60$ K which separates two different types of behavior of $H_{\text{res}}(T)$ and $\Delta H(T)$. At $T > T^*$, the resonance field is T -independent and it has the same value (within error bars) for both directions of H . The resonance condition $h\nu = g\mu_B H_{\text{res}}$ yields the isotropic g factor $g = 2.02$ for both compounds. It is close to the spin-only value of $g_S \approx 2.0023$, as expected for the Mn^{2+} ($S=5/2$, $L=0$) ion. In contrast, at $T < T^*$, H_{res} becomes significantly anisotropic. For $H \parallel ab$, the ESR line of MnBi_2Te_4 shifts slightly to higher fields, whereas for $H \parallel c$ it shifts strongly to smaller fields. Such behavior is typical for the antiferromagnetic (AFM) resonance modes [34]. However, these shifts commence well above $T_N \sim 24$ K and thus evidence the growth of the static, on the ESR time scale, short range Mn-Mn spin correlations already in the paramagnetic regime, which is typical for the intrinsically low-dimensional van der Waals magnets (see, e.g., Refs. [35, 36]). At $T < T_N$, the resonance line broadens and shifts further and finally disappears at $T \sim 17$ K since the AFM energy gap [34]

becomes larger than the microwave excitation energy $h\nu$ at $\nu = 9.56$ GHz. MnBi_4Te_7 exhibits at $T < T^*$ a qualitatively similar behavior [Fig. 1(e)]. In this case, the shifts are strong for both field geometries, typical for a ferromagnet with an easy axis anisotropy. Such ferromagnetic character of the low- T ESR response of MnBi_4Te_7 was established in our previous multifrequency ESR study [13].

The central observation in our ESR experiments is the contrasting behavior of the resonance line parameters in the high-temperature regime above $T^* \sim 60$ K. Here, an isotropic and T -independent value of the resonance field evidences an uncorrelated, paramagnetic state of the Mn spin system in both compounds. The linewidth follows a linear temperature dependence $\Delta H(T) = \Delta H_0 + bT$ [Figs. 1(d),(e)], characteristic of the Korringa relaxation of the localized magnetic moments by conduction electrons in the isothermal regime [37]. In this equation, ΔH_0 is the T -independent residual width due to, e.g., spin-spin interactions and magnetic field inhomogeneities, and the second term is the relaxation-driven T -dependent contribution [38]. Remarkably, for MnBi_2Te_4 , the Korringa slope $b = d\Delta H(T)/dT$ [37, 39] depends drastically on the direction of H . We obtain $b_c = 7.3 \pm 1$ Oe/K and $b_{ab} = 2.4 \pm 1$ Oe/K for $H \parallel c$ and $H \parallel ab$, respectively, yielding the ratio $b_{ab}/b_c = 0.33 \pm 0.14 \simeq 1/3$. In contrast, for MnBi_4Te_7 , the values $b_c = 9.3 \pm 0.5$ Oe/K and $b_{ab} = 8.6 \pm 0.5$ Oe/K are very close, with the ratio $b_{ab}/b_c = 0.92 \pm 0.07$. While the overall larger b values in MnBi_4Te_7 are probably due to a higher doping level [40], the very different anisotropy in the spin relaxation is more intriguing and will be discussed below.

Anisotropic Korringa relaxation. In a magnetic resonance experiment, one measures the components of the dynamical magnetization $M_{x,y}$ of the paramagnetic species at their resonance frequency [41, 42], transversal to the applied static magnetic field H . According to the so-called Bloch-Wangness-Redfield (BWR) theory, the width of the signal $\Delta H(T)$ is inversely proportional to the decay time τ of $M_{x,y}$ due to the relaxation processes caused by transversal and longitudinal fluctuating fields acting on the resonating spin ensemble [42–45]. In a metal, such fields are generated by conduction electrons exchange-coupled to the localized spins (s - d coupling). This mechanism, known as the Korringa relaxation [37, 39], gives rise to a linear in T increase of the linewidth and reads, in the simplest case, $\Delta H(T) \sim 1/\tau(T) \sim [JD(\varepsilon_F)]^2 T$ [38]. Here, $D(\varepsilon_F)$ is the density of states (DOS) of itinerant electrons at the Fermi energy ε_F and J is the s - d coupling strength. In ordinary metallic systems, the Korringa slope $b = d\Delta H(T)/dT$ is found to be rather independent of the direction of H . There are only a few known examples of anisotropic Korringa relaxation in systems containing heavy elements with strong spin-orbit coupling (SOC) [46–48]. These include OsF_6 -graphite intercalated compound, where the

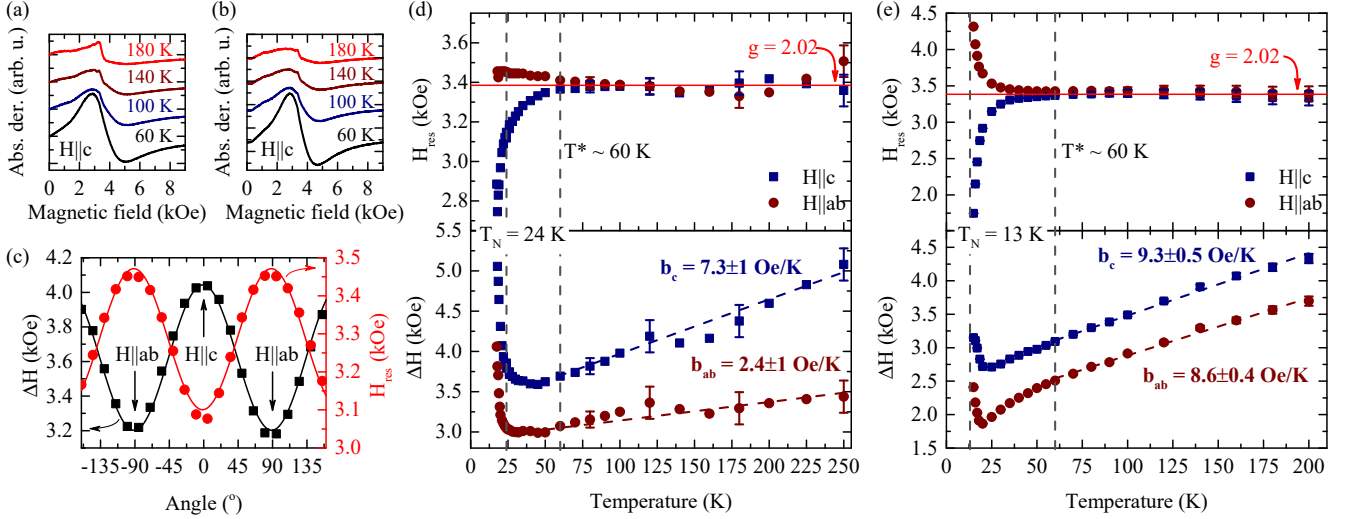


FIG. 1. ESR measurements. (a),(b) Temperature dependence of the spectra (field derivatives of the microwave absorption) with $H \parallel c$, for MnBi_2Te_4 and MnBi_4Te_7 , respectively. (c) Angular dependence of the linewidth ΔH and of the resonance field H_{res} at $T = 20$ K for MnBi_2Te_4 . Solid lines are fits of $\Delta H \sim [1 + \cos^2(\theta)]$ and $H_{\text{res}} \sim [1 + \sin^2(\theta)]$, where θ is the angle between H and the c axis; (d),(e) Temperature dependence of H_{res} and ΔH measured with two fields orientations for MnBi_2Te_4 and MnBi_4Te_7 , respectively. Dashed lines are fits of the Korringa dependence $\Delta H(T) = \Delta H_0 + bT$ while vertical dashed lines indicate the Néel temperature T_N and a crossover characteristic temperature T^* between two different types of temperature behavior of H_{res} and ΔH .

anisotropy was attributed to the anisotropy of J [46], and UPt_3 , where an anisotropic relaxation rate in a nuclear magnetic resonance experiment [47] was explained by the anisotropic fluctuations of the heavy-fermion spins. Notably, in both cases one finds the ratio of the Korringa slopes $b_{\text{ab}}/b_c \gtrsim 1/2$ [49]. In this respect, the significantly smaller ratio $b_{\text{ab}}/b_c \simeq 1/3$ found in MnBi_2Te_4 is unprecedented and remarkable.

To understand the sources of anisotropy in the Korringa relaxation, it is convenient to express the relaxation rate in terms of the frequency ω - and wave vector \mathbf{q} -dependent spin susceptibility $\chi_{i,i}(\omega, \mathbf{q})$ of conduction electrons, with $i = x, y, z$. Choosing the z axis along the direction of H , the relaxation rate reads [50, 51]

$$\frac{1}{\tau_z} = T \lim_{\omega \rightarrow 0} \frac{1}{\omega} \sum_{\mathbf{q}} \text{Im} [2 J_z^2 \chi_{zz}(\omega, \mathbf{q}) + \sum_{i=x,y} J_i^2 \chi_{ii}(\omega, \mathbf{q})], \quad (1)$$

where we have set $\hbar = k_B = 1$ and we have considered that the s - d exchange coupling consists of three different diagonal components J_i . An explicit calculation, see Supplementary Materials (SM) [52], yields

$$\frac{1}{\tau_z} = \pi T [2 J_z^2 |\mathcal{S}_z(\varepsilon_F)|^2 + \sum_{i=x,y} J_i^2 |\mathcal{S}_i(\varepsilon_F)|^2], \quad (2)$$

$$|\mathcal{S}_i(\varepsilon)|^2 = \sum_{\nu \mathbf{k}, \nu' \mathbf{k}'} \delta(\varepsilon - \varepsilon_{\nu \mathbf{k}}) \delta(\varepsilon - \varepsilon_{\nu' \mathbf{k}'}) |\mathcal{F}_{\mathbf{k} \mathbf{k}'}^{i, \nu \nu'}|^2, \quad (3)$$

where ν is a band index, \mathbf{k} the momentum and $|\mathcal{F}_{\mathbf{k} \mathbf{k}'}^{i, \nu \nu'}|^2$ denotes $\text{Tr}[\mathcal{F}_{\mathbf{k} \mathbf{k}'}^{i, \nu \nu'} \mathcal{F}_{\mathbf{k}' \mathbf{k}}^{i, \nu' \nu}]$, with $\mathcal{F}_{\mathbf{k} \mathbf{k}'}^{i, \nu \nu'} = \langle u_{\nu \mathbf{k}} | \hat{\sigma}_i | u_{\nu' \mathbf{k}'} \rangle / 2$

the matrix elements of the spin operator $\hat{\sigma}^i$ with respect to the spinor parts of Bloch functions $|u_{\nu \mathbf{k}}\rangle = a_{\nu \mathbf{k}} |\uparrow\rangle + b_{\nu \mathbf{k}} |\downarrow\rangle$. Without SOC, $\mathcal{F}_{\mathbf{k} \mathbf{k}'}^{i, \nu \nu'}$ is momenta-independent and, therefore, $\mathcal{S}_i(\varepsilon) \equiv D(\varepsilon)$. If we further consider an isotropic J , the original Korringa result is recovered [39]. In general, SOC can give rise to anisotropy both in J_i and in $\mathcal{S}_i(\varepsilon_F)$, which in turn may lead to anisotropic relaxation rates, as indicated by Eq. (2).

Eq. (2) was obtained in the zero magnetic field limit, which implies that the Larmor frequency of Mn spins ω_L is much smaller than the frequency of the spin fluctuations of the conduction electrons ω_{fl} . In this limit, Eq. (2) matches the BWR results expressing the fluctuating fields introduced in this theory as $\tau_0 \overline{H_i^2} = T J_i^2 |\mathcal{S}_i(\varepsilon_F)|^2$ (see SM [52]), where the correlation time τ_0 in our problem is $1/\omega_{\text{fl}}$. This connection provides a physical interpretation for the shape factors \mathcal{S}_i : They are the band structure property that together with T and J_i determine the effective magnetic field exerted by the electron cloud on the Mn spins on a timescale τ_0 . It further suggests an extension to the finite field case, $\omega_L \lesssim \omega_{\text{fl}}$, which in the BWR theory yields a pre-factor $\mathcal{A}_\omega \sim (1 + \omega_L^2/\omega_{\text{fl}}^2)^{-1}$ for the second term in Eq. (2) [42].

Given the layered structure of these compounds, J_c and \mathcal{S}_c can be significantly different from their in-plane counterparts $J_{\text{ab}}, \mathcal{S}_{\text{ab}}$ [53]. In this case, the ratio of the relaxation times reads

$$\frac{\tau_c}{\tau_{\text{ab}}} = \frac{1}{2} \frac{2 + \mathcal{A}_\omega(1 + \zeta)}{\mathcal{A}_\omega + \zeta}, \quad (4)$$

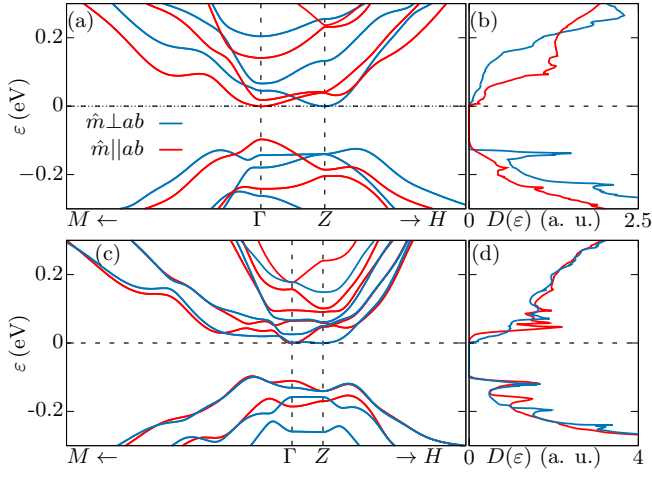


FIG. 2. (a),(b) Band structure and density of states, respectively, of MnBi_2Te_4 in the AFM phase for out-of-plane (blue) or in-plane (red) Mn magnetic moment direction. (c),(d) Analogous results for MnBi_4Te_7 .

where $\zeta = |J_c \mathcal{S}_c(\varepsilon_F)/J_{ab} \mathcal{S}_{ab}(\varepsilon_F)|^2$. If $\mathcal{S}_i(\varepsilon_F)$ is isotropic and $\omega_L/\omega_F \ll 1$, the remaining anisotropy due to that of J_i is bounded as $(1/2)J_{ab \rightarrow 0} < \tau_c/\tau_{ab} < (3/2)J_{c \rightarrow 0}$, posing a problem to account for the experimental result for MnBi_2Te_4 , $b_{ab}/b_c = \tau_c/\tau_{ab} \simeq 1/3$. Assuming a finite ratio ω_L/ω_F which yields $\mathcal{A}_\omega < 1$, the above limits can be surpassed, ultimately reaching $\tau_c/\tau_{ab} = 1/4$ for $\omega_L = \omega_F$ and $\zeta \gg 1$. However, that would require J to have an extreme Ising-like anisotropy with vanishing J_{ab} in MnBi_2Te_4 while being almost isotropic in MnBi_4Te_7 .

Therefore, to understand the anisotropy of the Korringa relaxation in MnBi_2Te_4 , it is necessary to analyze a possible anisotropy of the form factors $\mathcal{S}_i(\varepsilon_F)$ associated with the conduction electron cloud. This can be relevant when the carriers have a large SOC, as in the studied compounds. In such a case, for temperatures where the timescale of the dynamics of the Mn spins is longer than the timescale of conduction electrons, one may expect changes in the local electronic structure arising from the induced instantaneous polarization of the local moments, "frozen" on the fast electronic timescale, which can in turn affect the relaxation.

Band structure anisotropy. We now explore this idea, assuming a large separation between timescales: The measured ESR occurs on the slowest scale ($\sim 10^{-10}$ s); on the intermediate scale ($\sim 10^{-13} \dots 10^{-14}$ s), the Mn magnetic moment direction \hat{m} fluctuates; on the fast scale ($\sim 10^{-15}$ s), the electronic system adapts to the local Mn spin direction and dissipates the excitation. Figs. 2(a),(b) present the energy bands and DOS of MnBi_2Te_4 in the AFM phase for different \hat{m} , and Figs. 2(c),(d) show results for MnBi_4Te_7 [54]. The sensitivity to \hat{m} is significantly smaller in MnBi_4Te_7 . For this compound, within planes perpendicular to ΓZ , the bands are much less affected by \hat{m} , which naturally reflects in

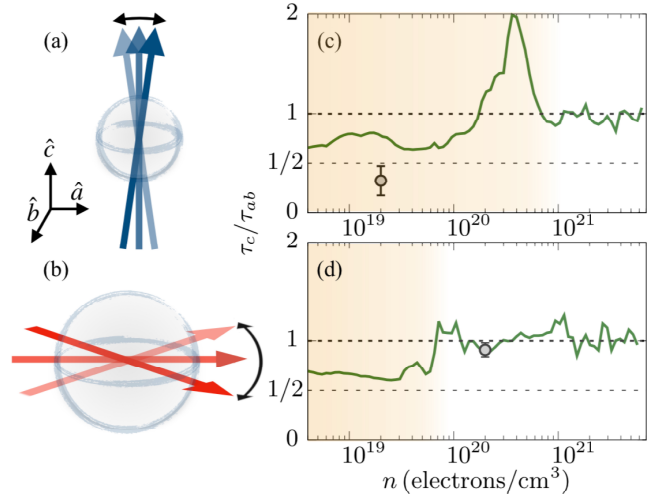


FIG. 3. (a,b) Pictorial representation of the anisotropic spin dynamics. An out-of-plane Mn spin is accompanied by a relatively small carriers DOS (gray electron cloud) and, accordingly, has a relatively slow dynamics as compared to an in-plane Mn spin, accompanied by a larger DOS and presenting faster dynamics. (c,d) Estimation of relaxation rate ratio as a function of the carrier density for MnBi_2Te_4 (c) and for MnBi_4Te_7 (d). The gray circles correspond to the experimental ESR data, estimating n from the Hall measurements on the same samples in Refs. [1] and [13], respectively.

$D(\varepsilon)$. Such lesser sensitivity possibly originates in various "dilution" effects caused by the Mn-free quintuple layer in MnBi_4Te_7 [52].

In MnBi_2Te_4 , for small electron doping, the DOS tends to be larger when $\hat{m}||ab$. This tendency qualitatively matches the results of the ESR experiment, where, for $H||c$, the in-plane part of the Mn dynamic magnetization $M_{x,y} = M_{a,b}$ is probed. For those Mn ions that have their spin essentially in-plane, the local electronic structure near them is better described by the calculation with $\hat{m}||ab$. The larger DOS in such case contributes to a faster relaxation rate of $M_{x,y}$ than in the configuration $H||ab$, where $M_{x,y} = M_{a,c} = M_{b,c}$ is probed [Figs. 3(a),(b)].

These ideas can be illustrated with the following ansatz for the shape factors [52]. We estimate them as $\mathcal{S}_i = \langle D_{ab}^2 \rangle$ for $H||c$ and as $\mathcal{S}_i = \langle D_{bc}^2 \rangle$ for $H||ab$, where $\langle D_{ij}^2 \rangle$ is the squared effective DOS when \hat{m} is along the direction i or j . Since the shape factors are defined by the electronic structure, it is worth stressing that the dependence on the direction of H does not come from the negligible H -dependence of the band structure. Rather, the role of H – together with the radio-frequency field direction – is to *select* the particular kind of fluctuations. For different directions of H , the measured resonance originates in Mn ions with different \hat{m} . The associated shape factors, considering the locally distinct electronic structure, are accordingly different.

Neglecting a possible anisotropy of J and assuming the limit $\omega_L/\omega_H \ll 1$, so that the effects described are purely related to the band structure, this approach yields $\tau_c/\tau_{ab} = \langle D_{bc}^2 \rangle / \langle D_{ab}^2 \rangle$. Figs. 3(c),(d) show the estimated ratio τ_c/τ_{ab} as a function of the carrier density n for MnBi_2Te_4 and MnBi_4Te_7 , respectively. Specifically, we consider $\langle D_{ab}^2 \rangle = D_{\tilde{m}|ab}^2$ and $\langle D_{bc}^2 \rangle = (D_{\tilde{m}|ab}^2 + D_{\tilde{m}|\tilde{c}}^2)/2$, where the DOS are evaluated at fixed n . For comparison, our experimental ESR results are included as gray circles. The almost isotropic Korringa relaxation in MnBi_4Te_7 is well captured, whereas the anisotropy in MnBi_2Te_4 is underestimated. However, quantitative agreement may be achieved by considering an anisotropy of J or a finite Larmor frequency, as discussed above.

Interestingly, both compounds exhibit a crossover as a function of doping signalled by large deviations from $\tau_c/\tau_{ab}=1$ at small n to nearly vanishing anisotropy at large n . It appears that the main difference between the compounds is the level of doping at which the crossover occurs. In particular, the samples of MnBi_2Te_4 and MnBi_4Te_7 lie on the anisotropic and isotropic sides of this crossover, respectively, in agreement with the ESR results. Reducing n in MnBi_4Te_7 by only one order of magnitude, potentially achievable by partial substitution of Bi by Sb [8], would recover the strong anisotropy $\tau_c < \tau_{ab}$, while a significant increase of n in MnBi_2Te_4 would change its type ($\tau_c > \tau_{ab}$) and eventually turn it to the isotropic limit ($\tau_c = \tau_{ab}$).

These results should be relevant for the interpretation of experiments in which the observed physical processes are not slow enough to average out the anisotropy of the Mn spin dynamics. This is for instance the case for the photoemission process in the non-adiabatic, sudden regime, which is typically associated with a timescale faster than 10^{-15} s. In particular, the much slower out-of-plane Mn spin dynamics in MnBi_2Te_4 indicates a larger out-of-plane dynamic polarization yielding a non zero instantaneous magnetic field perpendicular to the sample surface, which could contribute to the persistence of an electronic gap in the paramagnetic phase. Our theoretical results suggest that appropriate engineering of the carrier density can favor the opposite or vanishing anisotropy and hence, may provide a way to experimentally control the surface topological spectrum.

Conclusions. Our combined ESR and theoretical study shows that the Mn spin dynamics in magnetic topological insulators can be strongly anisotropic. The large spin-orbit coupling of conduction electrons plays a key role, making the local electronic structure strongly sensitive to Mn spin rotations, which in turn affects the Mn spin relaxation. Since the Mn spin dynamics can affect the topological surface states, our finding of the carrier density as a knob to control the anisotropy of magnetic fluctuations suggests a new way to tune the high-temperature surface spectrum of magnetic topological insulators. Altogether our results open a new per-

spective for exploring the magnetic dynamics and its interplay with non-trivial electronic structure in magnetic topological insulators and call for further investigations of the topological surface states at different time scales.

Acknowledgments. This work was financially supported by the Deutsche Forschungsgemeinschaft (DFG) through grant No. KA1694/12-1 and within the Collaborative Research Center SFB 1143 “Correlated Magnetism – From Frustration to Topology” (project-id 247310070) and the Dresden-Würzburg Cluster of Excellence (EXC 2147) “ct.qmat - Complexity and Topology in Quantum Matter” (project-id 39085490). J.I.F. acknowledges the support from the Alexander von Humboldt Foundation. K. M. acknowledges the Hallwachs–Röntgen Postdoc Program of ct.qmat for financial support. We thank Ulrike Nitzsche for technical assistance.

* These authors contributed equally to this work.

- [1] M. M. Otrokov, I. I. Klimovskikh, H. Bentmann, D. Esytunin, A. Zeugner, Z. S. Aliev, S. Gaß, A. U. B. Wolter, A. V. Koroleva, A. M. Shikin, M. Blanco-Rey, M. Hoffmann, I. P. Rusinov, A. Yu Vyazovskaya, S. V. Ere-meev, Yu M. Koroteev, V. M. Kuznetsov, F. Freyre, J. Sánchez-Barriga, I. R. Amiraslanov, M. B. Babanly, N. T. Mamedov, N. A. Abdullayev, V. N. Zverev, A. Al-fonsov, V. Kataev, B. Büchner, E. F. Schwier, S. Kumar, A. Kimura, L. Petaccia, G. Di Santo, R. C. Vidal, S. Schatz, K. Kikner, M. Ünzelmann, C. H. Min, Simon Moser, T. R. F. Peixoto, F. Reinert, A. Ernst, P. M. Echenique, A. Isaeva, and E. V. Chulkov, “Prediction and observation of an antiferromagnetic topological insulator,” *Nature* **576**, 416–422 (2019).
- [2] Yan Gong, Jingwen Guo, Jiaheng Li, Kejing Zhu, Menghan Liao, Xiaozhi Liu, Qinghua Zhang, Lin Gu, Lin Tang, Xiao Feng, *et al.*, “Experimental realization of an intrinsic magnetic topological insulator,” *Chinese Physics Letters* **36**, 076801 (2019).
- [3] Cui-Zu Chang, Jinsong Zhang, Xiao Feng, Jie Shen, Zuocheng Zhang, Minghua Guo, Kang Li, Yumbo Ou, Pang Wei, Li-Li Wang, Zhong-Qing Ji, Yang Feng, Shuaihua Ji, Xi Chen, Jinfeng Jia, Xi Dai, Zhong Fang, Shou-Cheng Zhang, Ke He, Yayu Wang, Li Lu, Xu-Cun Ma, and Qi-Kun Xue, “Experimental observation of the quantum anomalous hall effect in a magnetic topological insulator,” *Science* **340**, 167–170 (2013).
- [4] Qing Lin He, Lei Pan, Alexander L. Stern, Edward C. Burks, Xiaoyu Che, Gen Yin, Jing Wang, Biao Lian, Quan Zhou, Eun Sang Choi, Koichi Murata, Xufeng Kou, Zhijie Chen, Tianxiao Nie, Qiming Shao, Yabin Fan, Shou-Cheng Zhang, Kai Liu, Jing Xia, and Kang L. Wang, “Chiral majorana fermion modes in a quantum anomalous hall insulator–superconductor structure,” *Science* **357**, 294–299 (2017).
- [5] Yoshinori Tokura, Kenji Yasuda, and Atsushi Tsukazaki, “Magnetic topological insulators,” *Nature Reviews Physics* **1**, 126–143 (2019).
- [6] Jue Jiang, Di Xiao, Fei Wang, Jae-Ho Shin, Domenico Andreoli, Jianxiao Zhang, Run Xiao, Yi-Fan Zhao,

- Morteza Kayyalha, Ling Zhang, *et al.*, “Concurrence of quantum anomalous Hall and topological Hall effects in magnetic topological insulator sandwich heterostructures,” *Nature Materials*, 1–6 (2020).
- [7] Yujun Deng, Yijun Yu, Meng Zhu Shi, Zhongxun Guo, Zihan Xu, Jing Wang, Xian Hui Chen, and Yuanbo Zhang, “Quantum anomalous Hall effect in intrinsic magnetic topological insulator MnBi_2Te_4 ,” *Science* **367**, 895–900 (2020).
- [8] Bo Chen, Fucong Fei, Dongqin Zhang, Bo Zhang, Wanling Liu, Shuai Zhang, Pengdong Wang, Boyuan Wei, Yong Zhang, Zewen Zuo, *et al.*, “Intrinsic magnetic topological insulator phases in the Sb doped MnBi_2Te_4 bulks and thin flakes,” *Nature communications* **10**, 1–8 (2019).
- [9] Daniel Souchay, Markus Nentwig, Daniel Günther, Simon Keilholz, Johannes de Boor, Alexander Zeugner, Anna Isaeva, Michael Ruck, Anja UB Wolter, Bernd Büchner, *et al.*, “Layered manganese bismuth tellurides with GeBi_4Te_7 - and $\text{GeBi}_6\text{Te}_{10}$ -type structures: towards multifunctional materials,” *Journal of Materials Chemistry C* **7**, 9939–9953 (2019).
- [10] J.-Q. Yan, Q. Zhang, T. Heitmann, Zengle Huang, K. Y. Chen, J.-G. Cheng, Weida Wu, D. Vaknin, B. C. Sales, and R. J. McQueeney, “Crystal growth and magnetic structure of MnBi_2Te_4 ,” *Phys. Rev. Materials* **3**, 064202 (2019).
- [11] Lei Ding, Chaowei Hu, Feng Ye, Erxi Feng, Ni Ni, and Huibo Cao, “Crystal and magnetic structures of magnetic topological insulators MnBi_2Te_4 and MnBi_4Te_7 ,” *Phys. Rev. B* **101**, 020412 (2020).
- [12] Jiazhen Wu, Fucai Liu, Masato Sasase, Koichiro Ienaga, Yukiko Obata, Ryu Yukawa, Koji Horiba, Hiroshi Kumigashira, Satoshi Okuma, Takeshi Inoshita, and Hideo Hosono, “Natural van der Waals heterostructural single crystals with both magnetic and topological properties,” *Science Advances* **5** (2019), 10.1126/sciadv.aax9989.
- [13] Raphael C. Vidal, Alexander Zeugner, Jorge I. Facio, Rajyavardhan Ray, M. Hossein Haghighi, Anja U. B. Wolter, Laura T. Corredor Bohorquez, Federico Cagliaris, Simon Moser, Tim Figgemeier, Thiago R. F. Peixoto, Hari Babu Vasili, Manuel Valvidares, Sungwon Jung, Cephise Cacho, Alexey Alfonsov, Kavita Mehlaawat, Vladislav Kataev, Christian Hess, Manuel Richter, Bernd Büchner, Jeroen van den Brink, Michael Ruck, Friedrich Reinert, Hendrik Bentmann, and Anna Isaeva, “Topological Electronic Structure and Intrinsic Magnetization in MnBi_4Te_7 : A Bi_2Te_3 Derivative with a Periodic Mn Sublattice,” *Phys. Rev. X* **9**, 041065 (2019).
- [14] Chaowei Hu, Kyle N Gordon, Pengfei Liu, Jinyu Liu, Xiaoping Zhou, Peipei Hao, Dushyant Narayan, Eve Emmanouilidou, Hongyi Sun, Yuntian Liu, *et al.*, “A van der Waals antiferromagnetic topological insulator with weak interlayer magnetic coupling,” *Nature communications* **11**, 1–8 (2020).
- [15] Roger S. K. Mong, Andrew M. Essin, and Joel E. Moore, “Antiferromagnetic topological insulators,” *Phys. Rev. B* **81**, 245209 (2010).
- [16] I. C. Fulga, B. van Heck, J. M. Edge, and A. R. Akhmerov, “Statistical topological insulators,” *Phys. Rev. B* **89**, 155424 (2014).
- [17] Kevin F. Garrity, Sugata Chowdhury, and Francesca M. Tavazza, “Topological surface states of MnBi_2Te_4 at finite temperatures and at domain walls,” arXiv e-prints, arXiv:2003.03439 (2020), [arXiv:2003.03439](https://arxiv.org/abs/2003.03439) [cond-mat.mtrl-sci].
- [18] R. C. Vidal, H. Bentmann, T. R. F. Peixoto, A. Zeugner, S. Moser, C.-H. Min, S. Schatz, K. Kifner, M. Ünzelmann, C. I. Fornari, H. B. Vasili, M. Valvidares, K. Sakamoto, D. Mondal, J. Fujii, I. Vobornik, S. Jung, C. Cacho, T. K. Kim, R. J. Koch, C. Jozwiak, A. Bostwick, J. D. Denlinger, E. Rotenberg, J. Buck, M. Hoesch, F. Diekmann, S. Rohlf, M. Kalläne, K. Rossnagel, M. M. Otrokov, E. V. Chulkov, M. Ruck, A. Isaeva, and F. Reinert, “Surface states and Rashba-type spin polarization in antiferromagnetic $\text{MnBi}_2\text{Te}_4(0001)$,” *Phys. Rev. B* **100**, 121104 (2019).
- [19] Yu-Jie Hao, Pengfei Liu, Yue Feng, Xiao-Ming Ma, Eike F. Schwier, Masashi Arita, Shiv Kumar, Chaowei Hu, Rui’e Lu, Meng Zeng, Yuan Wang, Zhanyang Hao, Hong-Yi Sun, Ke Zhang, Jiawei Mei, Ni Ni, Liusuo Wu, Kenya Shimada, Chaoyu Chen, Qihang Liu, and Chang Liu, “Gapless Surface Dirac Cone in Antiferromagnetic Topological Insulator MnBi_2Te_4 ,” *Phys. Rev. X* **9**, 041038 (2019).
- [20] Hang Li, Shun-Ye Gao, Shao-Feng Duan, Yuan-Feng Xu, Ke-Jia Zhu, Shang-Jie Tian, Jia-Cheng Gao, Wen-Hui Fan, Zhi-Cheng Rao, Jie-Rui Huang, Jia-Jun Li, Da-Yu Yan, Zheng-Tai Liu, Wan-Ling Liu, Yao-Bo Huang, Yuliang Li, Yi Liu, Guo-Bin Zhang, Peng Zhang, Takeshi Kondo, Shik Shin, He-Chang Lei, You-Guo Shi, Wen-Tao Zhang, Hong-Ming Weng, Tian Qian, and Hong Ding, “Dirac Surface States in Intrinsic Magnetic Topological Insulators EuSn_2As_2 and $\text{MnBi}_{2n}\text{Te}_{3n+1}$,” *Phys. Rev. X* **9**, 041039 (2019).
- [21] Y. J. Chen, L. X. Xu, J. H. Li, Y. W. Li, H. Y. Wang, C. F. Zhang, H. Li, Y. Wu, A. J. Liang, C. Chen, S. W. Jung, C. Cacho, Y. H. Mao, S. Liu, M. X. Wang, Y. F. Guo, Y. Xu, Z. K. Liu, L. X. Yang, and Y. L. Chen, “Topological Electronic Structure and Its Temperature Evolution in Antiferromagnetic Topological Insulator MnBi_2Te_4 ,” *Phys. Rev. X* **9**, 041040 (2019).
- [22] Przemyslaw Swatek, Yun Wu, Lin-Lin Wang, Kyungchan Lee, Benjamin Schunk, Jiaqiang Yan, and Adam Kaminski, “Gapless Dirac surface states in the antiferromagnetic topological insulator MnBi_2Te_4 ,” *Phys. Rev. B* **101**, 161109 (2020).
- [23] Yong Hu, Lixuan Xu, Mengzhu Shi, Aiyun Luo, Shuting Peng, Z. Y. Wang, J. J. Ying, T. Wu, Z. K. Liu, C. F. Zhang, Y. L. Chen, G. Xu, X.-H. Chen, and J.-F. He, “Universal gapless Dirac cone and tunable topological states in $(\text{MnBi}_2\text{Te}_4)_m(\text{Bi}_2\text{Te}_3)_n$ heterostructures,” *Phys. Rev. B* **101**, 161113 (2020).
- [24] Kyle N Gordon, Hongyi Sun, Chaowei Hu, A Garrison Linn, Haoxiang Li, Yuntian Liu, Pengfei Liu, Scott Mackey, Qihang Liu, Ni Ni, *et al.*, “Strongly Gapped Topological Surface States on Protected Surfaces of Antiferromagnetic MnBi_4Te_7 and $\text{MnBi}_6\text{Te}_{10}$,” *arXiv preprint arXiv:1910.13943* (2019).
- [25] Ilya I. Klimovskikh, Mikhail M. Otrokov, Dmitry Estyunin, Sergey V. Ereemeev, Sergey O. Filnov, Alexandra Koroleva, Eugene Shevchenko, Vladimir Voroshnin, Artem G. Rybkin, Igor P. Rusinov, Maria Blanco-Rey, Martin Hoffmann, Ziya S. Aliev, Mahammad B. Babanly, Imamaddin R. Amiraslanov, Nadir A. Abdullayev, Vladimir N. Zverev, Akio Kimura, Oleg E. Tereshchenko, Konstantin A. Kokh, Luca Petaccia, Giovanni Di Santo, Arthur Ernst, Pedro M. Echenique, Nazim T. Mamedov, Alexander M. Shikin, and Eugene V. Chulkov, “Tunable

- 3d/2d magnetism in the (mnbi2te4)(bi2te3)m topological insulators family,” *npj Quantum Materials* **5**, 54 (2020).
- [26] LX Xu, YH Mao, HY Wang, JH Li, YJ Chen, YYY Xia, YW Li, J Zhang, HJ Zheng, K Huang, *et al.*, “Persistent gapless surface states in MnBi₂Te₄/Bi₂Te₃ superlattice antiferromagnetic topological insulator,” *arXiv preprint arXiv:1910.11014* (2019).
- [27] Xuefeng Wu, Jiayu Li, Xiao-Ming Ma, Yu Zhang, Yuntian Liu, Chun-Sheng Zhou, Jifeng Shao, Qiaoming Wang, Yu-Jie Hao, Yue Feng, Eike F. Schwier, Shiv Kumar, Hongyi Sun, Pengfei Liu, Kenya Shimada, Koji Miyamoto, Taichi Okuda, Kedong Wang, Maohai Xie, Chaoyu Chen, Qihang Liu, Chang Liu, and Yue Zhao, “Distinct topological surface states on the two terminations of mnbi₄te₇,” *Phys. Rev. X* **10**, 031013 (2020).
- [28] R. C. Vidal, H. Bentmann, J. I. Facio, P. Kagerer, C. I. Fornari, T. R. F. Peixoto, T. Figgemeier, S. Jung, C. Cacho, B. Büchner, J. van den Brink, E. F. Schwier, K. Shimada, M. Richter, A. Isaeva, and F. Reinert, “Orbital Complexity in Intrinsic Magnetic Topological Insulators MnBi₄Te₇ and MnBi₆Te₁₀,” (2020), *arXiv:2007.07637 [cond-mat.str-el]*.
- [29] A. M. Shikin, D. A. Estyunin, I. I. Klimovskikh, S. O. Filnov, E. F. Schwier, S. Kumar, K. Miyamoto, T. Okuda, A. Kimura, K. Kuroda, K. Yaji, S. Shin, Y. Takeda, Y. Saitoh, Z. S. Aliev, N. T. Mamedov, I. R. Amirasanov, M. B. Babanly, M. M. Otrokov, S. V. Ereemeev, and E. V. Chulkov, “Nature of the Dirac gap modulation and surface magnetic interaction in axion antiferromagnetic topological insulator MnBi₂Te₄,” *Scientific Reports* **10**, 13226 (2020).
- [30] Alexander Zeugner, Frederik Nietschke, Anja U. B. Wolter, Sebastian Gaß, Raphael C. Vidal, Thiago R. F. Peixoto, Darius Pohl, Christine Damm, Axel Lubk, Richard Hentrich, Simon K. Moser, Celso Fornari, Chul Hee Min, Sonja Schatz, Katharina Kißner, Maximilian Ünzelmann, Martin Kaiser, Francesco Scaravaggi, Bernd Rellinghaus, Kornelius Nielsch, Christian Hess, Bernd Büchner, Friedrich Reinert, Hendrik Bentmann, Oliver Oeckler, Thomas Doert, Michael Ruck, and Anna Isaeva, “Chemical Aspects of the Candidate Antiferromagnetic Topological Insulator MnBi₂Te₄,” *Chemistry of Materials* **31**, 2795–2806 (2019).
- [31] George Feher and A. F. Kip, “Electron Spin Resonance Absorption in Metals. I. Experimental,” *Phys. Rev.* **98**, 337–348 (1955).
- [32] Freeman J. Dyson, “Electron Spin Resonance Absorption in Metals. II. Theory of Electron Diffusion and the Skin Effect,” *Phys. Rev.* **98**, 349–359 (1955).
- [33] Aoyu Tan, Valentin Labracherie, Narayan Kunchur, Anja U. B. Wolter, Joaquin Cornejo, Joseph Dufouleur, Bernd Büchner, Anna Isaeva, and Romain Giraud, “Metamagnetism of Weakly Coupled Antiferromagnetic Topological Insulators,” *Phys. Rev. Lett.* **124**, 197201 (2020).
- [34] E. A. Turov, *Physical Properties of Magnetically Ordered Crystals*, edited by A. Tybulewicz and S. Chomet (Academic Press, New York, 1965).
- [35] J. Zeisner, A. Alfonsov, S. Selter, S. Aswartham, M. P. Ghimire, M. Richter, J. van den Brink, B. Büchner, and V. Kataev, “Magnetic anisotropy and spin-polarized two-dimensional electron gas in the van der Waals ferromagnet Cr₂Ge₂Te₆,” *Phys. Rev. B* **99**, 165109 (2019).
- [36] J. Zeisner, K. Mehawat, A. Alfonsov, M. Roslova, T. Doert, A. Isaeva, B. Büchner, and V. Kataev, “Electron spin resonance and ferromagnetic resonance spectroscopy in the high-field phase of the van der Waals magnet CrCl₃,” *Phys. Rev. Mater.* **4**, 064406 (2020).
- [37] S.E. Barnes, “Theory of electron spin resonance of magnetic ions in metals,” *Advances in Physics* **30**, 801–938 (1981).
- [38] The linear in temperature Korringa relaxation is the unique fingerprint of the relaxation of the localized *d*-states via the exchange coupling to the conduction electrons. Other relaxation channels are either *T*-independent (e.g dipole-dipole or exchange interactions) or strongly non-linear in *T* (spin-phonon relaxation) [41]. The latter mechanism is inactive for Mn²⁺ due to the absence of the orbital moment.
- [39] J. Korringa, “Nuclear magnetic relaxation and resonance line shift in metals,” *Physica* **16**, 601 – 610 (1950).
- [40] This is supported by the difference in the room temperature resistivity values ρ for these compounds: MnBi₂Te₄ has $\rho \sim 1.5 \text{ m}\Omega\text{cm}$ [1] and MnBi₄Te₇ has $\rho \sim 0.31 \text{ m}\Omega\text{cm}$ [13].
- [41] A. Abragam and B. Bleaney, *Electron paramagnetic resonance of transition ions* (Oxford University Press, Oxford, 2012).
- [42] C.P. Slichter, *Principles of Magnetic Resonance*, Springer Series in Solid-State Sciences (Springer Berlin Heidelberg, 1996).
- [43] R. K. Wangsness and F. Bloch, “The Dynamical Theory of Nuclear Induction,” *Phys. Rev.* **89**, 728–739 (1953).
- [44] F. Bloch, “Dynamical Theory of Nuclear Induction. II,” *Phys. Rev.* **102**, 104–135 (1956).
- [45] A. G. Redfield, “On the Theory of Relaxation Processes,” *IBM J. Res. Dev.* **1**, 19–31 (1957).
- [46] D. Vaknin, D. Davidov, V. Zevin, and H. Selig, “Anisotropy and two-dimensional effects in the ESR properties of OsF₆-graphite intercalation compounds,” *Phys. Rev. B* **35**, 6423–6431 (1987).
- [47] J. P. Vithayathil, D. E. MacLaughlin, E. Koster, D. Ll. Williams, and E. Bucher, “Spin fluctuations and anisotropic nuclear relaxation in single-crystal UPt₃,” *Phys. Rev. B* **44**, 4705–4708 (1991).
- [48] V Kataev, U Schaufuß, F Murányi, A Alfonsov, M Doerr, M Rotter, and B Büchner, “Magnetic anisotropy of the spin-antiferromagnet GdNi₂B₂C probed by high-frequency ESR,” *Journal of Physics: Conference Series* **150**, 042086 (2009).
- [49] Note, that for the OsF₆-GIC this ratio $b_{ab}/b_c \gtrsim 1/2$ is still true if the g-factor anisotropy, present in this compound, is not taken into account.
- [50] T. Moriya, “The effect of electron-electron interaction on the nuclear spin relaxation in metals,” *Journal of the Physical Society of Japan* **18**, 516–520 (1963).
- [51] R. E. Walstedt and A. Narath, “Relaxation of local-moment nuclei in metals,” *Phys. Rev. B* **6**, 4118–4125 (1972).
- [52] See Supplementary Materials for: (i) derivation of Eq. 2, (ii) a discussion on the shape factors and (iii) further details on the DFT results.
- [53] We neglect anisotropy within the *ab* plane in all discussions and calculations.
- [54] Fully relativistic calculations in the Generalized Gradient Approximation+U (atomic limit) were performed using the FPLO code version 18.52 with parameters $U = 2 \text{ eV}$ and $J = 1 \text{ eV}$. We used a linear tetrahedron method with *k*-meshes of $24 \times 24 \times 24$ (rhombohedral setup) and $22 \times$

22×4 (hexagonal setup) subdivisions for MnBi_2Te_4 and MnBi_4Te_7 , respectively. To compute the DOS, we used in each case meshes of up to $60 \times 60 \times 60$ subdivisions and $60 \times 60 \times 5$. Structural details are based on experimental lattice parameters, see Refs. [1] and [13].

SUPPLEMENTARY MATERIAL

Details on the theory of ESR for spin-orbit coupled systems

Following the well-established theory of NMR, when the static field is applied along z -axis, the spin relaxation rate can be expressed as [50, 51]

$$\frac{1}{\tau_z} = \frac{\gamma^2}{4} \int dt \cos \omega_L t \langle \{ \delta B_+(t), \delta B_-(0) \} \rangle + \frac{\gamma^2}{2} \int dt \langle \{ \delta B_z(t), \delta B_z(0) \} \rangle, \quad (5)$$

in terms of the fluctuating internal field $\delta \mathbf{B}$ acting on the local moment. Here γ denotes the gyromagnetic ratio, $\omega_L = \gamma H_{\text{res}}$ is the resonance frequency, $\hat{A}, \hat{B} = \hat{A}\hat{B} + \hat{B}\hat{A}$ is the anticommutator of two operators, and finally $\langle \hat{A} \rangle = \text{Tr}(\rho_{\text{th}} \hat{A})$ denotes the statistical average of the operator. Also the field is decomposed as $\delta \mathbf{B} = \delta B_+ \hat{\mathbf{e}}_- + \delta B_- \hat{\mathbf{e}}_+ + \delta B_z \hat{\mathbf{e}}_z$ with $\delta B_{\pm} = \delta B_x \pm i \delta B_y$ and $\hat{\mathbf{e}}_{\pm} = (\hat{\mathbf{e}}_x \pm i \hat{\mathbf{e}}_y)/2$. Notice that $\hat{\mathbf{e}}_{\pm}$ and $\hat{\mathbf{e}}_z$ also create an orthogonal coordinate frame.

We consider a bath of noninteracting conduction fermions $\mathcal{H}_0 = \sum_{\nu \mathbf{k}} \varepsilon_{\nu \mathbf{k}} c_{\nu \mathbf{k}}^\dagger c_{\nu \mathbf{k}}$, where $\varepsilon_{\nu \mathbf{k}}$ are the energy bands of the corresponding Bloch wavefunctions $|\psi_{\nu \mathbf{k}}\rangle = e^{i \mathbf{k} \cdot \mathbf{r}} |u_{\nu \mathbf{k}}\rangle$. These fermions are coupled with a local moment \mathbf{S} via a general anisotropic s - d exchange coupling, which reads

$$\mathcal{H}_{\text{ex}} = \sum_{\mathbf{q}} \mathbf{S} \cdot \mathbf{J} \cdot \hat{\mathbf{s}}_{\mathbf{q}} = \sum_{ij, \mathbf{q}} J_{ij} S^i \hat{s}_{\mathbf{q}}^j, \quad \text{with } \hat{s}_{\mathbf{q}}^j = \frac{1}{2} \sum_{\mathbf{k}, s, s'} c_{\mathbf{k}+\mathbf{q}, s}^\dagger \sigma_{ss'}^j c_{\mathbf{k}, s'} \quad (6)$$

Here, we omit, for brevity, the band index. The fluctuating fields due to the electronic cloud around the local moments and in terms of electron creation and annihilation field operators, read

$$\widehat{\delta B}_{\pm} = \frac{1}{\gamma} \sum_{j, \mathbf{q}} J_{\pm, j} \hat{s}_{\mathbf{q}}^j = \frac{1}{\gamma} \sum_{j, \mathbf{q}} (J_{x, j} \pm i J_{y, j}) \hat{s}_{\mathbf{q}}^j \quad (7)$$

$$\widehat{\delta B}_z = \frac{1}{\gamma} \sum_{j, \mathbf{q}} J_{z, j} \hat{s}_{\mathbf{q}}^j \quad (8)$$

Inserting above expressions in Eq. 5, we find:

$$\frac{1}{\tau_z} = \frac{1}{4} \sum_{i, j} J_{+, i} J_{-, j} \int dt \cos \omega_L t \sum_{\mathbf{q}} \langle \{ \hat{s}_{\mathbf{q}}^i(t), \hat{s}_{-\mathbf{q}}^j \} \rangle + \frac{1}{2} \sum_{i, j} J_{z, i} J_{z, j} \int dt \sum_{\mathbf{q}} \langle \{ \hat{s}_{\mathbf{q}}^i(t), \hat{s}_{-\mathbf{q}}^j \} \rangle \quad (9)$$

Using the symmetry of the anticommutator, $\langle \{ \hat{s}_{\mathbf{q}}^i(t), \hat{s}_{-\mathbf{q}}^j \} \rangle = \langle \{ \hat{s}_{-\mathbf{q}}^j(-t), \hat{s}_{\mathbf{q}}^i \} \rangle$, and noting that $\frac{J_{+, i} J_{-, j} + J_{-, i} J_{+, j}}{2} = J_{x, i} J_{x, j} + J_{y, i} J_{y, j}$ the relaxation time reads

$$\frac{1}{\tau_z} = T \sum_{i, j} (J_{x, i} J_{x, j} + J_{y, i} J_{y, j} + 2 J_{z, i} J_{z, j}) \times \lim_{\omega \rightarrow 0} \frac{1}{\omega} \sum_{\mathbf{q}} \text{Im } \chi_{ij}(iq_n, \mathbf{q})|_{iq_n \rightarrow \omega + i0^+} \quad (10)$$

To obtain this equation, we have used the quantum-mechanical version of fluctuation-dissipation theorem defining the spin susceptibility tensor $\chi(iq_n, \mathbf{q})$ with components $\chi_{ij}(iq_n, \mathbf{q})$. This relation is valid for large enough temperature $T \gg \omega_L$. Note that we have set the Planck and Boltzmann constant as $\hbar = k_B = 1$. The spin susceptibility in Matsubara representation is

$$\chi_{ij}(iq_n, \mathbf{q}) = -\frac{T}{4} \sum_{ik_n, \mathbf{k}} \text{Tr} [\hat{\sigma}^i \hat{G}(ik_n, \mathbf{k}) \hat{\sigma}^j \hat{G}(ik_n + iq_n, \mathbf{k} + \mathbf{q})], \quad (11)$$

with bosonic and fermionic Matsubara frequencies denoted as $q_n = 2n\pi T$ and $k_n = (2n+1)\pi T$, respectively. The noninteracting Green's function can be generally written as

$$\hat{G}(ik_n, \mathbf{k}) = \sum_{\nu} \frac{|u_{\nu \mathbf{k}}\rangle \langle u_{\nu \mathbf{k}}|}{ik_n - \varepsilon_{\nu \mathbf{k}}}. \quad (12)$$

We can readily arrive at the following suitable expression for the susceptibility

$$\chi_{ij}(iq_n, \mathbf{q}) = -\frac{T}{4} \sum_{ik_n, \mathbf{k}} \sum_{\nu \nu'} \text{Tr} [\mathcal{F}_{\mathbf{k}, \mathbf{k}+\mathbf{q}}^{i, \nu \nu'} \mathcal{F}_{\mathbf{k}+\mathbf{q}, \mathbf{k}}^{j, \nu' \nu}] \times \frac{1}{(ik_n - \varepsilon_{\nu \mathbf{k}})(ik_n + iq_n - \varepsilon_{\nu', \mathbf{k}+\mathbf{q}})}, \quad (13)$$

with $\mathcal{F}_{\mathbf{k}\mathbf{k}'}^{i,\nu\nu'} = \langle u_{\nu\mathbf{k}} | \hat{\sigma}^i | u_{\nu'\mathbf{k}'} \rangle / 2$. Then by performing the Matsubara sum we find

$$\frac{1}{\tau_z} = -\pi T \sum_{i,j} (J_{x,i} J_{x,j} + J_{y,i} J_{y,j} + 2 J_{z,i} J_{z,j}) \sum_{\mathbf{k},\mathbf{q},\nu,\nu'} \delta(\varepsilon_{\nu\mathbf{k}} - \varepsilon_{\nu'\mathbf{k}+\mathbf{q}}) \left. \frac{\partial n(\omega)}{\partial \omega} \right|_{\omega=\varepsilon_{\nu\mathbf{k}}} \text{Tr}[\mathcal{F}_{\mathbf{k},\mathbf{k}+\mathbf{q}}^{i,\nu\nu'} \mathcal{F}_{\mathbf{k}+\mathbf{q},\mathbf{k}}^{j,\nu'\nu}]. \quad (14)$$

Considering diagonal exchange coupling terms $J_{ij} = J_i \delta_{ij}$, defining $\text{Tr}[\mathcal{F}_{\mathbf{k}\mathbf{k}'}^{i,\nu\nu'} \mathcal{F}_{\mathbf{k}'\mathbf{k}}^{i,\nu'\nu}] = |\mathcal{F}_{\mathbf{k}\mathbf{k}'}^{i,\nu\nu'}|^2$ and replacing the derivative of Fermi-Dirac distribution $n(\omega)$ with its zero temperature value, this simplifies to

$$\frac{1}{\tau_z} = \pi T \sum_{\nu\mathbf{k},\nu'\mathbf{k}'} \delta(\varepsilon_{\nu\mathbf{k}} - \varepsilon_{\nu'\mathbf{k}'}) \delta(\varepsilon_F - \varepsilon_{\nu\mathbf{k}}) \times \left(J_x^2 |\mathcal{F}_{\mathbf{k}\mathbf{k}'}^{x,\nu\nu'}|^2 + J_y^2 |\mathcal{F}_{\mathbf{k}\mathbf{k}'}^{y,\nu\nu'}|^2 + 2 J_z^2 |\mathcal{F}_{\mathbf{k}\mathbf{k}'}^{z,\nu\nu'}|^2 \right), \quad (15)$$

which is the result presented in Eq. 2 and 3 of the main text.

On the shape factors \mathcal{S}_i

Here, first, for completeness, we recall the essential results from the Bloch-Wangness-Redfield (BWR) theory; and second, we further motivate the approximation proposed for the shape factors \mathcal{S}_i . The BWR theory analyzes the relaxation phenomena in an ensemble of magnetic moments subject to a random magnetic field $H_j(t)$, with $j = x, y, z$ [42]. Considering the external static field H along \hat{z} and the external radiofrequency field H_{rf} within the xy plane, the relaxation time results

$$\frac{1}{\tau_z} = \gamma^2 \left(\tau_0 \overline{H_z^2} + \frac{1}{2} \frac{\tau_0}{1 + \omega_L^2 \tau_0^2} (\overline{H_x^2} + \overline{H_y^2}) \right). \quad (16)$$

Here, τ_0 and $\overline{H_j^2}$ characterize the correlation in time of the random forces, $\overline{H_j(t)H_j(t+\tau)} = \overline{H_j^2} \exp(-\tau/\tau_0)$. The asymmetric appearance of the different field components in Eq. 16 can be traced to their different role, which roughly speaking can be thought of as randomizing the Larmor frequency (the z -component) or the radiofrequency field (the xy components).

In our case, the random magnetic fields are given by the exchange with conduction electrons [Eqs. 7,8] and τ_0 can be related with the frequency of the spin fluctuations of these electrons, $\tau_0 \sim 1/\omega_{fl}$. As shown in Section (I), while these random magnetic fields naturally depend on the crystal momentum of the carriers, their net effect on the relaxation rate is encoded in integral properties of the band structure – the shape factors \mathcal{S}_i . A comparison of Eqs. 2 and 3 of the main text with Eq. 16 suggests the identification $\tau_0 \overline{H_j^2} = T J_j^2 \mathcal{S}_j^2$, which provides a simple physical interpretation: the effective magnetic field exerted by the conduction electronic cloud over the timescale τ_0 is determined by the s - d exchange, the temperature and the shape factors \mathcal{S}_i .

Our DFT results indicate that due to the spin-orbit coupling the electronic structure, e.g. the density of states, presents a strong sensitivity to the direction of the Mn magnetic moments \hat{m} . The ansatz for the shape factors proposed in the main text aims to describe how such sensitivity can in turn affect the local moment relaxation process. Notice that strictly speaking, such effects are absent in Eq. 15 since correlations between the conduction electrons and the magnetic moments were neglected.

While a complete theory is beyond the scope of this work, a heuristic motivation for the ansatz presented in the main text is based on the following considerations. First, one considers that due to the spin-orbit coupling the instantaneous magnetic field exerted by the conduction electron cloud on the Mn moments depends on \hat{m} . Defining an instantaneous shape factor $s_j(t, \hat{m})$, one has

$$T J_j^2 \mathcal{S}_j^2 = T J_j^2 \int_0^{\tau_{ce}} dt s_j(t, \hat{m}), \quad (17)$$

where τ_{ce} is the timescale associated with conducting electrons, typically $\sim \hbar/W$, with W their bandwidth. Second, the timescale of Mn spin fluctuations is assumed to be *larger* than τ_{ce} and naturally smaller than τ_z . In this intermediate timescale local rotations of \hat{m} are followed essentially instantaneously by the electron cloud. Third, out of the ensemble of fluctuating Mn spins, a given configuration of H and H_{rf} picks up only certain components of the dynamical magnetization. For instance, for $H \parallel c$ and $H_{\text{rf}} \parallel ab$, the measured relaxation originates in the in-plane component of the dynamical magnetization. Thus, we assume the electron cloud near the contributing Mn moments – and, in turn, the exerted magnetic field – to be better described by the electronic structure with in-plane magnetic moments.

Last, an argument for the estimation of the shape factor as the DOS computed for different \hat{m} is based on considering the effects of the SOC perturbatively. At zero order, $\mathcal{S}_i^2 \propto D^2(\varepsilon_F)$. At first order, the matrix elements in $|\mathcal{F}_{\mathbf{k}\mathbf{k}'}^{i,\nu\nu'}|^2$ in

Eq. 15 are unaffected and the only effect on \mathcal{S}_i^2 is caused by the change in the eigenenergies. This change reflects in the electronic DOS in a manner that depends on the magnetic moment orientation. Our ansatz, $\mathcal{S}_i^2 \propto D^2(\varepsilon_F)|_{\hat{m} \perp H}$, can be thought of as using this first-order perturbation theory result replacing the DOS with the one computed with DFT for different \hat{m} .

Details of the DFT results

On the different electronic structure anisotropy of MnBi_2Te_4 and MnBi_4Te_7

To further understand the origin of the different sensitivity of the density of states of MnBi_2Te_4 and MnBi_4Te_7 to the orientation of the magnetic moments, here we consider the projection of the density of states on different atoms in the unit cell. For brevity, we define $\Delta = D_{\mathbf{m}||ab} - D_{\mathbf{m}||c}$. The key structural difference between these compounds is the additional quintuple layer (QL) in MnBi_4Te_7 . One could, therefore, suspect that the contribution to the Bloch states of the atoms in the QL could be less sensitive to \hat{m} than the contribution of the atoms in the septuple layer (SL). The additional QL would, therefore, act to reduce (by diluting) the overall sensitivity of the total density of states. Fig. 5(a) shows the projection of Δ on the QL (named Δ^{QL}) and on the SL (Δ^{SL}) and it can be seen that in the range of energies $[0.1, 0.3]$ eV, $|\Delta^{\text{QL}}| < |\Delta^{\text{SL}}|$. The difference are, however, rather modest. More significant than this is the effect that the additional QL has on the sensitivity of the SL contribution. To illustrate this, Fig. 5(b) shows the projection of Δ on the Bi atoms in the SL, both for MnBi_2Te_4 (Δ_{124}^{Bi}) and MnBi_4Te_7 (Δ_{147}^{Bi}). It can be seen that $|\Delta_{124}^{\text{Bi}}|$ is significantly larger than $|\Delta_{147}^{\text{Bi}}|$. A similar reduction is found in the projection on the Te atoms in the SL (not shown).

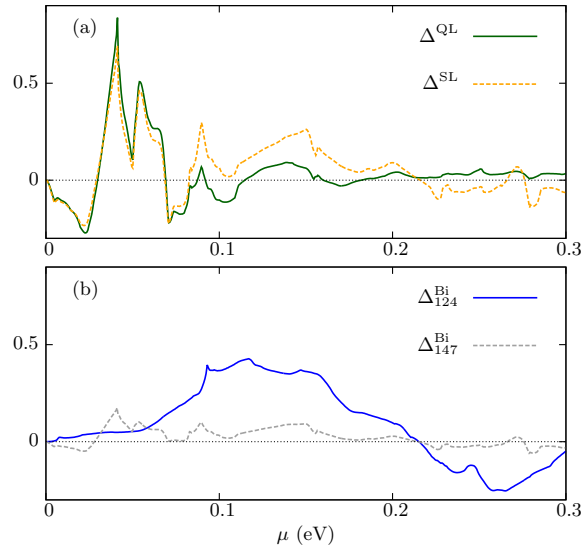


FIG. 4. Δ is the difference between the density of states corresponding to the cases $\hat{m}||ab$ and $\hat{m}||c$. (a) For MnBi_4Te_7 , projection of Δ on the quintuple and sextuple layers. (b) For MnBi_2Te_4 and MnBi_4Te_7 , projection of Δ on the Bi atoms in the septuple layer.

Carriers density vs Fermi energy.

For the estimation of τ_c/τ_{ab} as a function of the carrier density n , we consider the involved DOS at fixed n . For this, we first compute n as a function of the Fermi energy ε_F . These curves, shown in Fig. 5 also make very transparent the sensitivity of the electronic structure to the direction of the magnetic moments \hat{m} . While both compounds present a strong anisotropy at sufficient small doping, the main difference lies in the level of doping required to make the anisotropy negligible. While for MnBi_4Te_7 this occurs at small doping ($\mu \sim 50\text{meV}$, $n \sim 5 \times 10^{19}$ electron/cm³), for MnBi_2Te_4 the anisotropy is preserved in a broader range of doping, which includes all estimates based on Hall-data reported in the literature.

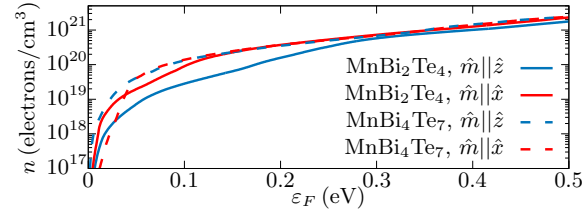


FIG. 5. Carrier density n vs Fermi energy ε_F for MnBi_2Te_4 and MnBi_4Te_7 , for different orientations of the magnetic moments.